



Shape-controlled synthesis of monolithic ZSM-5 zeolite with hierarchical structure and mechanical stability

Deju Wang^{a,b,1}, Zhongneng Liu^{b,1}, Hui Wang^{b,1}, Zaiku Xie^{b,1}, Yi Tang^{a,*}

^a Department of Chemistry, Shanghai Key Laboratory of Molecular Catalysis and Innovative Materials and Laboratory of Advanced Materials, Fudan University, Shanghai 200433, People's Republic of China

^b Shanghai Research Institute of Petrochemical Technology, SINOPEC, Shanghai 201208, People's Republic of China

ARTICLE INFO

Article history:

Received 18 October 2009

Received in revised form 17 February 2010

Accepted 22 March 2010

Available online 27 March 2010

Keywords:

ZSM-5 zeolite monolith

Hierarchical porosity

Hollow structure

Hydrothermal transformation

Catalysis

ABSTRACT

Columned ZSM-5 zeolite monoliths with hierarchical structure and excellent mechanical strength were successfully prepared by a hydrothermal transformation method. The pre-formed extrudates of aluminosilicate embedded with β zeolite were subjected to a hydrothermal synthesis system and the hierarchical porous ZSM-5 zeolite monoliths with the same columned shape were obtained after the hydrothermal treatment. The intra-particle hollow structure formed during hydrothermal synthesis was attributed to the digestion of inner β zeolite accompanying with the growth of ZSM-5 zeolite shell. The related data of X-ray diffraction (XRD), scanning electron microscopy (SEM), Fourier transform infrared (FT-IR) analysis, N_2 -sorption experiment and mercury intrusion porosimetry (MIP), showed ZSM-5 zeolite monolith had enriched multi-porosity and excellent mechanical stability, which contribute to its further application in field of catalysis and separation. The obtained hierarchical ZSM-5 zeolite monoliths showed superior catalytic performance in α -pinene isomerization for their proper acidity and good diffusion, compared with the ZSM-5 zeolite sample prepared from the precursor without β zeolite.

© 2010 Published by Elsevier Inc.

1. Introduction

Zeolite molecular sieves are widely used in the fields of adsorption, separation and catalysis due to their uniform and ordered micropores, large specific surface area and high hydrothermal stability [1]. A multitude of chemical reactions are catalyzed by zeolites including Y, β , ZSM-5 and mordenite, which often exhibit unique properties of both activity and selectivity. However, the intrinsic molecular-sized micropores of zeolite have diffusional limitations on the chemical reaction rate as well as catalytic performance. To facilitate the diffusion of reactant/product in bulky molecule-involved and/or diffusion-controlled catalytic reactions, some efforts have been devoted to hierarchical porous zeolite materials with meso- and/or macro-porosity [2,3]. As one of such typical structures, mesoporous zeolites were generally fabricated by extraction the framework elements of zeolite [4,5] or through assembling zeolite nanocrystals on the mesoscaled templates [6,7]. Additionally, zeolite materials with bimodal pore structure of micro- and macro-pores were successfully fabricated by the means of pseudosolid-state transformation [8] or self-assembly

of colloidal zeolites [9,10] using polystyrene microspheres as templates. Another approach to fabricate zeolite structures with hollow cavities was done through secondary growth combining the removal of inorganic or organic templates [11,12]. Besides of these, the hollow zeolite structures could also be obtained by chemical conversion of the zeolite-seeded silica spheres [13,14], alkali dissolution [15,16] and re-crystallization [17] of the zeolite crystals.

Although the insertion of meso- and macro-pores into zeolitic materials has great improvement of the diffusivity in catalytic application, as-synthesized zeolite crystals are conventionally obtained in fine powder form. As in the case of industrial catalysis, a certain amount of binders, such as alumina, silica, clay, etc. are generally used for cementing zeolite crystals into large sticks or granules with mechanical stability. However, the inorganic binders may dilute the active zeolite and partially block the pore system, which give rise to diffusion limitation and inaccessibility of the active species. To overcome these problems, continuous progress is made on the mechanical stable zeolite monoliths with both uniform shape and hierarchical structure. Such monolithic zeolite material facilitates not only practical preparation and application, but also reactant/product diffusion as well as reaction efficiency [18,19]. In past developed strategies, a technique of gel-casting for shaping nanozeolite into designed macroscopic structure was well performed to get silicalite-1 tube with hierarchical porosity [20]. And the self-organization or growth of zeolite crystals on

* Corresponding author. Tel.: +86 21 55664125; fax: +86 21 65641740.

E-mail addresses: djwang@sript.com.cn (D. Wang), yitang@fudan.edu.cn (Y. Tang).

¹ Tel.: +86 21 68462197; fax: +86 21 68462283.

the removable organic templates has been prepared for zeolite monoliths with uniform morphologies [18,21–24]. Other than assembly the zeolite into monoliths, directly crystallization of the prefabricated reactive aluminosilicate could produce well structured zeolite monoliths with hierarchical porosity. The chemical transformation of the zeolite-seeded silica spheres to hollow zeolite capsules was extended to prepare three-dimensionally ordered macroporous zeolite monoliths [25,26]. Closely packed ZSM-5 and beta nanocrystalline assemblies were also prepared from amorphous silica grains using the homologous methods [27,28]. Recently, through vapor-phase transport (VPT) conversion of the pre-formed diatomite containing aluminosilicate precursors, the zeolite monoliths of ultrafine ZSM-5 crystals were successfully fabricated, which possessing enriched porosity and good mechanical stability [29].

In this work, in order to develop the practical application of zeolite materials, hierarchical porous ZSM-5 zeolite monoliths with uniform macroscopical shape and excellent mechanical strength has been prepared by facile hydrothermal treatment, using the pre-formed extrudates of aluminosilicate embedded with β zeolite as starting material. This method allows the gradual transformation of the aluminosilicate adjacent to β zeolite into the ZSM-5 zeolite. During this process, the inner β zeolite was almost digested as the nutrient for the growth of outer ZSM-5 zeolite, forming an interesting intra-particle hollow structure within the monoliths. As a result, the whole pre-formed extrudates were converted into the intergrown ZSM-5 zeolite materials. The method demonstrated here is facile and convenient for mass production. The resulted ZSM-5 zeolite monolithic materials with abundant hierarchical porosity and uniform macroscopic morphologies would be widely used as much more efficient catalyst and adsorbent. In the present study, the catalytic performance in α -pinene isomerization was also investigated using the protonated zeolite samples as catalyst.

2. Experimental

2.1. Zeolite monoliths preparation

The chemicals including tetrapropylammonium bromide (TPABr), NaOH, silica sol ($\text{SiO}_2 = 40 \text{ wt.}\%$), fumed silica, $\text{NaAlO}_2 \cdot x\text{H}_2\text{O}$ ($\text{Al}_2\text{O}_3 \geq 41 \text{ wt.}\%$), deionized water were commercially phased and used without further purification. A commercial β zeolite with $\text{SiO}_2/\text{Al}_2\text{O}_3$ molar ratio of about 20 and the Brunauer–Emmett–Teller (BET) surface area of $526.3 \text{ m}^2 \text{ g}^{-1}$ is used, which has high crystallinity and the irregular morphological agglomerate with the size around $0.8\text{--}2.0 \mu\text{m}$ (Fig. 1).

The fabrication of hierarchical porous ZSM-5 zeolite monoliths generally involved preparation of the β zeolite-embedded alumi-

nosilicate extrudates followed by the hydrothermal transformation process. The β zeolite-containing aluminosilicate extrudates were typically prepared as follows: 160 g of β zeolite powder, 50 g of $\text{NaAlO}_2 \cdot x\text{H}_2\text{O}$ and 200 g of fumed silica were well mixed, and then 600 g of silica sol (40 wt.%) were added therein. Then the mixtures were kneaded and extruded into cylindrical shaped extrudates with diameter of 1.5 mm. After drying at 110°C , the extrudates was calcined in air at 550°C for 4 h, denoted as 8100. Then 20 g of the extrudates (8100) and 50 g of a mixture solution of NaOH: TPABr: $1178\text{H}_2\text{O}$ were put in a PTFE-lined stainless steel autoclave. The autoclaves were then enclosed and heated at 160°C . After crystallization for 48 and 72 h, the resulting products were washed with distilled water, dried, and calcined in air at 550°C for 4 h, denoted as 8148-CB and 8172-CB, respectively. For a reference study, the aluminosilicate extrudates without β zeolite were treated under the same hydrothermal conditions for 72 h and the product was denoted as R72.

2.2. Characterization

XRD patterns for phase identification were collected with a Rigaku D/max-IIA diffractometer with $\text{Cu-K}\alpha$ radiation at 40 kV and 30 mA. SEM was carried out on a Philips XL30 electron microscope to examine the morphology and the size of the crystalline samples. The transmission FT-IR spectra in KBr pellets were recorded using a Bruker IFS88 spectrometer at a spectral resolution of 4 cm^{-1} . The N_2 -sorption isotherms and specific surface areas were determined by nitrogen physisorption at liquid-nitrogen temperature using a Micromeritics Tristar 3000 automatic analyzer. The macropore size distributions were analyzed by MIP using a Micromeritics Poresizer 9320.

2.3. Catalytic performance assessment

The catalytic performance of the protonated 8172-CB and R72 was evaluated by the batch isomerization of α -pinene. A mixture of 6 g of α -pinene and 0.2 g of zeolite sample was added to a bottle and the reaction was carried out in the sealed bottle with a magnetic stirrer at 105°C . The products were analyzed by a gas chromatograph equipped with a flame ionization detector.

3. Results and discussion

The XRD patterns of the calcined extrudates (8100) and the products (8148-CB and 8172-CB) are shown in Fig. 2. The pattern of 8100 has a wide dispersive peak of amorphous aluminosilicate at $15\text{--}30^\circ$ besides the diffraction peaks of β zeolite, indicating that β zeolite is the sole crystalline phase in the calcined extrudates

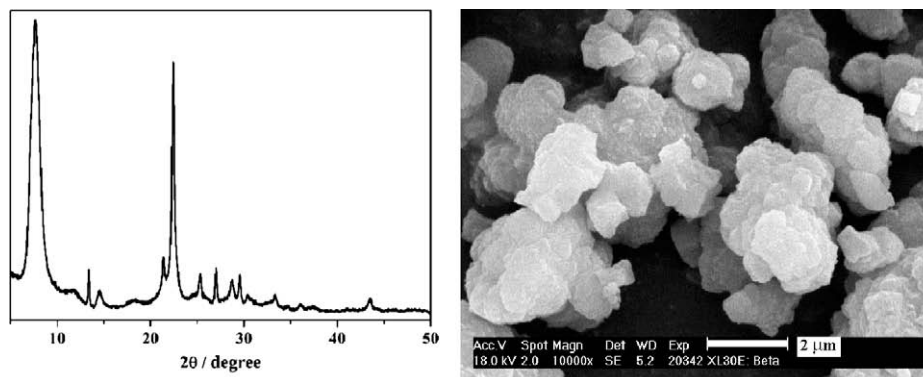


Fig. 1. XRD pattern and SEM image of β zeolite nanocrystals.

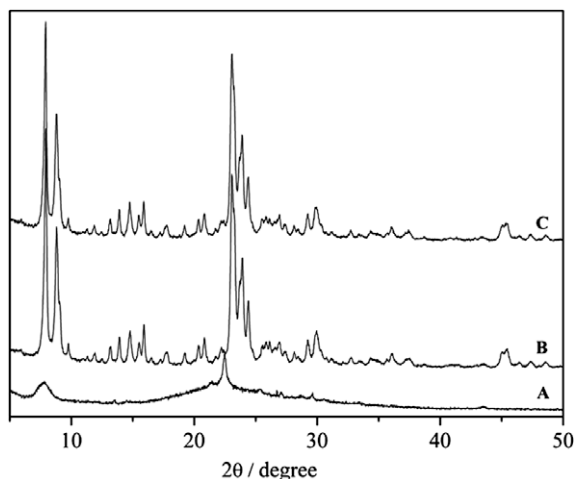


Fig. 2. XRD patterns of the aluminosilicate extrudates 8100 (A), the products of 8148-CB (B) and 8172-CB (C).

(Fig. 2a). Fig. 3 is the SEM images of the calcined sample 8100 after kneading and extrusion. The shaped precursor of 8100 shows an impacted structure and almost no β zeolite morphologies but tiny granules could be observed, indicating that the β zeolite crystals have been completely wrapped by the amorphous aluminosilicate during the shaping process.

After hydrothermal crystallization for 2 and 3 days, the XRD patterns (Fig. 2b and c) showed the sharp diffraction peaks belong-

ing to MFI zeolite. Both of the diffraction peaks of β zeolite and the dispersive peak at 15–30° of amorphous aluminosilicate disappear completely. The products 8148-CB and 8172-CB have almost the same intensities of XRD peaks of MFI zeolite. These data demonstrated that the amorphous aluminosilicate and β zeolite in 8100 have all been converted into ZSM-5 zeolite during hydrothermal process. The final products well kept the initial cylindrical shape of the precursor (Fig. 4) and possessed excellent mechanical strength. The compressive strength of 8148-CB and 8172-CB is larger than that of 8100 (Table 1), which might result from the intergrowth of the ZSM-5 zeolite crystals. The produced zeolite monoliths with such good mechanical strength are rigid enough for various applications especially for the industrial catalysis and separation.

From the SEM images of the final products 8148-CB and 8172-CB (Fig. 5A and D), the intergrown spherical particles were clearly observed on the surfaces of the cylindrical products. Interestingly, most of the particles are found to be hollow from the SEM images of cross-section (Fig. 5B and E), which should be attributed to the digestion of the inner β zeolite during the crystallization process. Because the β zeolite nanocrystals added are instable in aqueous alkali solution at high temperature [30], they should be extracted as the nutrients for the growth of outer ZSM-5 zeolite during the hydrothermal process. It is consistent with the disappearance of the β zeolite peaks in the XRD patterns of products (Fig. 2). The growth of ZSM-5 zeolite depends on both the extraction nutrients from the inner β zeolite and the surrounding aluminosilicate in the extrudates, which result in the hollow zeolite structure. Additionally, the enriched macro-porosity could be observed among the

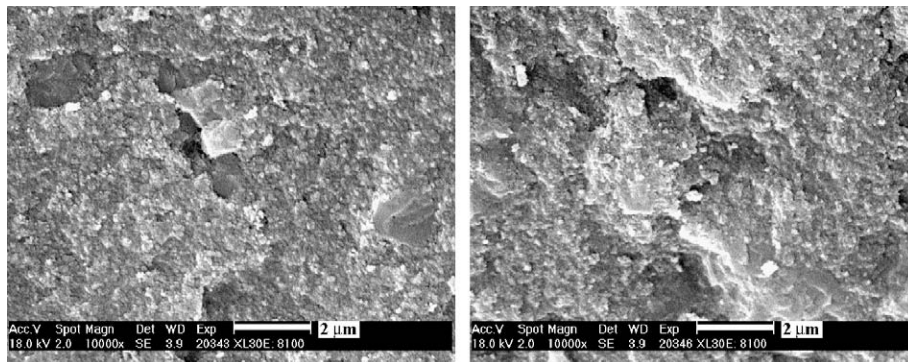


Fig. 3. SEM images of the aluminosilicate extrudates 8100.

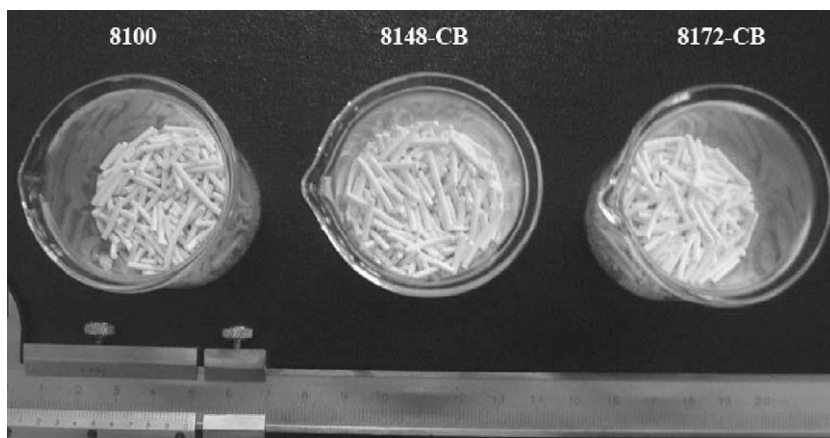


Fig. 4. Photograph of the precursory extrudates and the zeolite products.

Table 1

Texture and mechanical properties of the precursor and the products of zeolite monoliths.

Samples	Surface area ($\text{m}^2 \text{g}^{-1}$)			Pore volume ($\text{cm}^3 \text{g}^{-1}$)		Compressive strength	
	S_{BET}	S_{Mic}	$S_{\text{Ext}}^{\text{a}}$	$V_{\text{Mic}}^{\text{a}}$	$V_{\text{Meso}}^{\text{a}}$	Radial (N cm^{-1})	Axial (MPa)
8100	159.2	83.9	75.3	0.04	0.34	≥ 98.4	≥ 17.0
8148-CB	321.7	254.9	66.8	0.12	0.06	≥ 135.0	≥ 22.6
8172-CB	324.9	257.2	67.7	0.12	0.06	≥ 160.0	≥ 22.6
R72	294.6	235.8	58.8	0.12	0.06	–	–

^a Determined by *t*-plot according to the method of Lepens and de Boer [20].

intergrown zeolite particles, which are probably caused by consuming silica–alumina during the intergrowth of zeolite (Fig. 5C and F). From the SEM images of cross-section, the spherical particles in the inner part of the cylindrical products are composed of tiny zeolite granules with the size ($\sim 200 \text{ nm}$, Fig. 5C and F) smaller than the crystals on the surfaces of the cylindrical products (Fig. 5A and D). It may be due to that TPABr and NaOH could diffuse into the interior of the cylindrical extrudates for the crystallization of the inside aluminosilicate, so that the TPABr and NaOH concentrations on the surface are higher than those in the inner region. As the result, a higher growth rate of ZSM-5 occurs on the surface than the interior of the extrudates. Moreover, some cores of aggre-

gated rod-like crystals were still observed inside some of the hollow cavities in the SEM images at high magnification (Fig. 6). These cores would be aggregations of ZSM-5 nanocrystals for their typical coffin-like crystal morphology of MFI zeolite. They may come from the transformation of the β zeolite particles with relative large size which cannot be completely digested. This was also proved by the disappearance of the diffraction peaks of β zeolite in the XRD pattern (Fig. 2). The conversion process was also tracked by FT-IR spectroscopy, as shown in Fig. 7. The gradual transformation of the β zeolite into ZSM-5 structure was additionally proved by the simultaneous fade-up of a characteristic MFI band at 550 cm^{-1} and fade-down of β zeolite band at 565 cm^{-1} with the

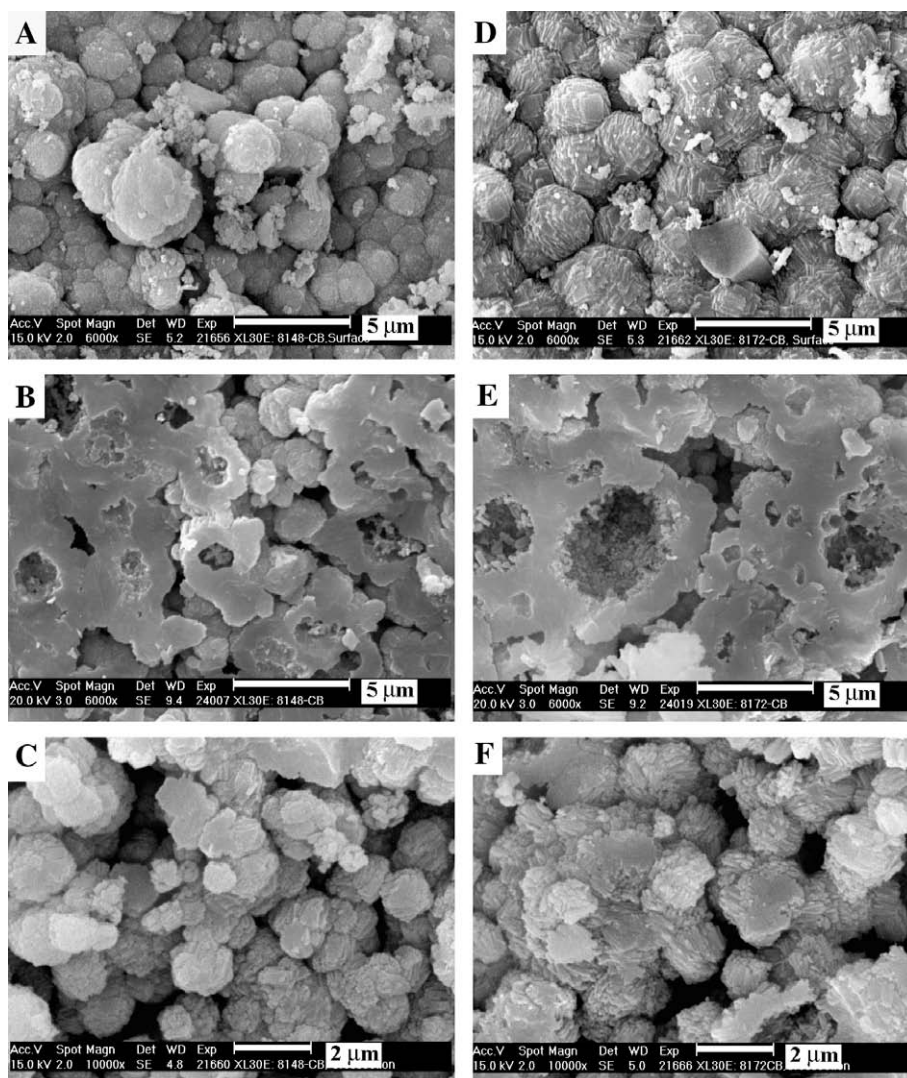


Fig. 5. SEM images of the products. (A) surface and (B) and (C) cross-section of 8148-CB; (D) surface and (E) and (F) cross-section of 8172-CB.

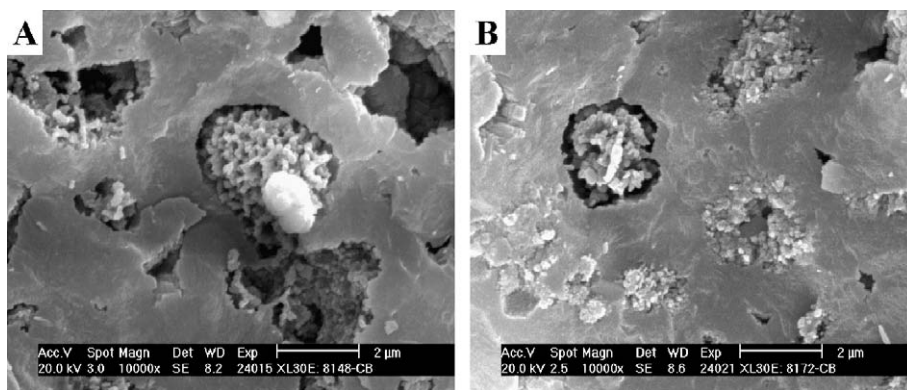


Fig. 6. SEM images of the aggregation small ZSM-5 zeolite crystals inside the hollow cavities. (A) 8148-CB and (B) 8172-CB.

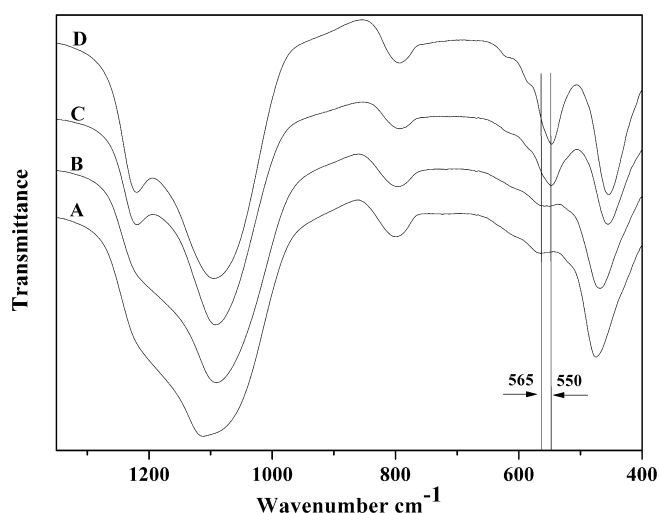


Fig. 7. FT-IR spectra of the calcined precursory extrudates (A) and the products after (B) 12, (C) 24 and (D) 48 h hydrothermal treatment.

prolonging of the crystallization time [31,32]. When the crystallization time reaching 48 h, the band at 565 cm^{-1} assigned to the five-membered rings in the β zeolite tended to disappear, indicated β zeolite was almost converted. From the quantitative XRD analyses (wt.%) of samples based on Rietveld Refinement using Topas software, the contents of β zeolite in 8148-CB was 2.1%, whereas none of β zeolite in 8172-CB. The increase of the zeolite species in the hydrothermal process was also demonstrated by the progressive development of the zeolite structure-sensitive asymmet-

ric stretch vibration for external linkages at 1221 cm^{-1} [33,34]. Zeolite β was employed as a precursor of other zeolites in several researches [35–37], which demonstrated enhanced nucleation, increased reaction rates, greater flexibility in the choice of template and possibilities for lattice substitution [35]. In our work, it is proposed that the metastable β zeolite could be converted into steady MFI zeolite structure in the presence of TPA^+ at high temperature, because the kinetic control is a pervading influence throughout zeolite synthesis [35,38]. For the aluminosilicate extrudates without β zeolite, a well crystalline ZSM-5 sample R72 was also obtained after 72 h crystallization (Fig. 8, inset). However, most of R72 sample was cracked pieces and the initial cylindrical shape of the precursor could not be kept well. Moreover, no hollow structure was found in the existing integrated R72 sample from the SEM image of cross-section (Fig. 8B), which further proved the hollow structures in 8148-CB and 8172-CB formed from the digestion of the β zeolite during the crystallization process. This implies the addition of the β zeolite in precursors may improve the mechanical stability of the final hierarchical ZSM-5 zeolite monoliths.

Fig. 9 is N_2 adsorption–desorption isotherms of the ZSM-5 zeolite monoliths of 8148-CB and 8172-CB as well as 8100, and their texture properties are presented in Table 1. The BET specific surface area and micropore volume (t -plot method [39]) of the products 8148-CB and 8172-CB are much larger than those of the precursor 8100, further proving the formation of the microporous ZSM-5 zeolite. The micropores creation and the mesopores shrinkage after the hydrothermal treatment was evident from their N_2 adsorption–desorption isotherms (Fig. 9). The 8148-CB and 8172-CB samples display a slight uptake of nitrogen and a small hysteresis loop at higher relative pressures of $P/P_0 > 0.45$, indicating the existence of some mesopores. The external surface area of the 8148-CB and 8172-CB products is a little smaller than that of the precursor 8100, but the mesopore volume of the products is only

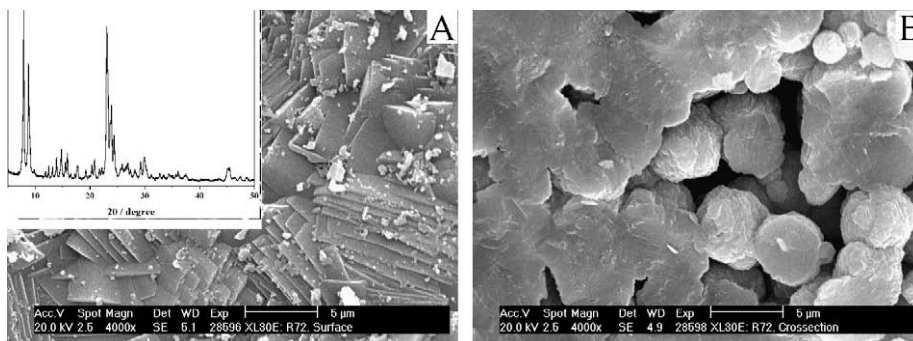


Fig. 8. SEM images of R72 sample: (A) surface and (B) cross-section. The inset shows the XRD pattern of R72.

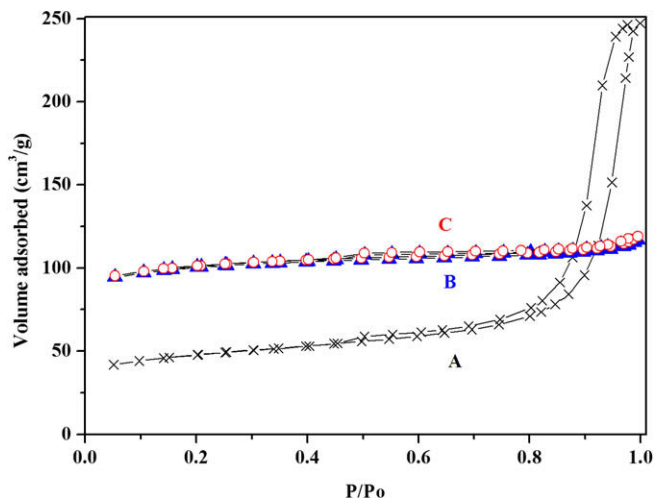


Fig. 9. N_2 adsorption–desorption isotherms (77 K) for (A) 8100, (B) 8148-CB and (C) 8172-CB.

$0.06 \text{ cm}^3 \text{ g}^{-1}$, much smaller than $0.34 \text{ cm}^3 \text{ g}^{-1}$ of the precursor 8100. These facts may imply that the increase of the amount of mesopore but decrease of the mesopore size in the 8148-CB and 8172-CB products ($r = 2 \text{ V/S}$). As compared, R72 has lower specific surface area than 8172-CB but almost the same micro-/mesopore volume (Table 1).

The macro-pores of the zeolite monoliths come from the apertures among the zeolite particles, as well as the void spaces from the hollow structure (Fig. 5). The mercury intrusion curves and the macropore size distributions (PSD) of the products and precursor extrudates are shown in Fig. 10 as the function of pore diameter. The ZSM-5 zeolite monoliths of 8148-CB and 8172-CB have the size of macropore diameter in the range of 60–2000 nm and present a bimodal pore size distribution with maxima at 900 and 450 nm. However, their precursor 8100 is of great difference from the products. There are almost no macro-pores with diameters larger than 30 nm in precursor 8100. This can be confirmed from the

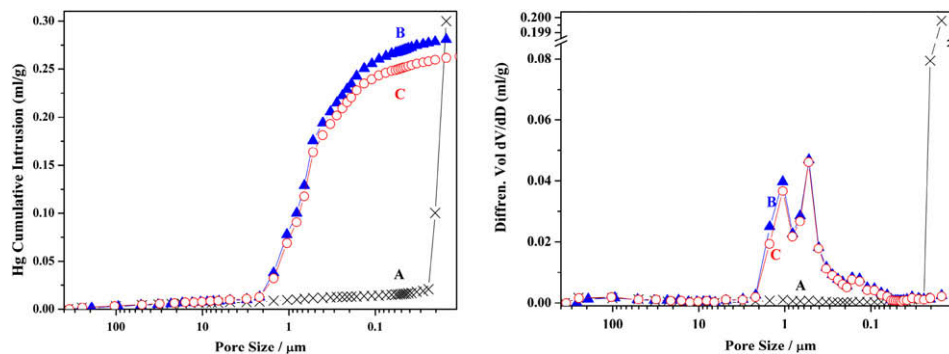


Fig. 10. Hg intrusion and pore size distribution (PSD) of samples calculated from MIP (A) 8100, (B) 8148-CB and (C) 8172-CB.

Table 2

Texture properties of the samples from the mercury intrusion porosimetry data.

Samples	Total intrusion volume ($\text{cm}^3 \text{ g}^{-1}$)	Total pore area ($\text{m}^2 \text{ g}^{-1}$)	Average pore diameter (μm)	Bulk density (g cm^{-3})	Skeletal density (g cm^{-3})	Porosity (%)	Stem volume used ^a (%)
8100	0.32	78.00	0.02	1.24	2.08	40.15	40.00
8148-CB	0.28	5.58	0.20	1.19	1.79	33.65	34.00
8172-CB	0.26	5.10	0.21	1.23	1.82	32.42	32.00

^a A value of the stem volume between 25–90% demonstrates that the analyses are reliable.

average pore diameter calculated in Table 2, which increased from 20 up to 200 and 210 nm from 8100 to 8148-CB and 8172-CB. Accordingly, the total intrusion volume and pore area decreased. It should be noted that the MIP data spans the measurement of pore sizes ranging from a few nanometers to several hundred micrometers. The MIP porosity and surface area usually reflects the macro-pores and some mesopores in the materials. The creation of the macro-pores in the monolithic zeolite columns is due to the dissolution of β zeolite and re-crystallization of the surrounding aluminosilicate into ZSM-5 zeolite, which results in the large apertures among the zeolite particles and the void spaces of the hollow structure. Consequently the ZSM-5 monoliths with hierarchical porosity of micro/meso/macro-pores are obtained through the facile hydrothermal conversion of the β zeolite-containing extrudates.

The isomerization of α -pinene is commonly catalyzed using acid catalysts. In this study, α -pinene isomerization was used as model

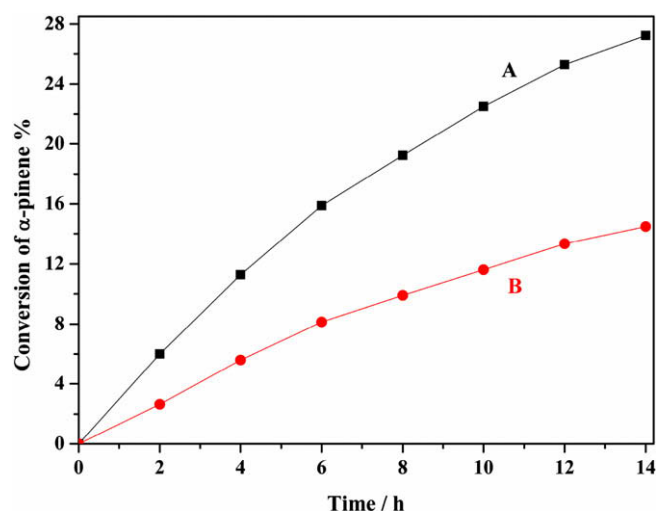


Fig. 11. Results of α -pinene isomerization over (A) H-8172-CB and (B) H-R72 catalysts.

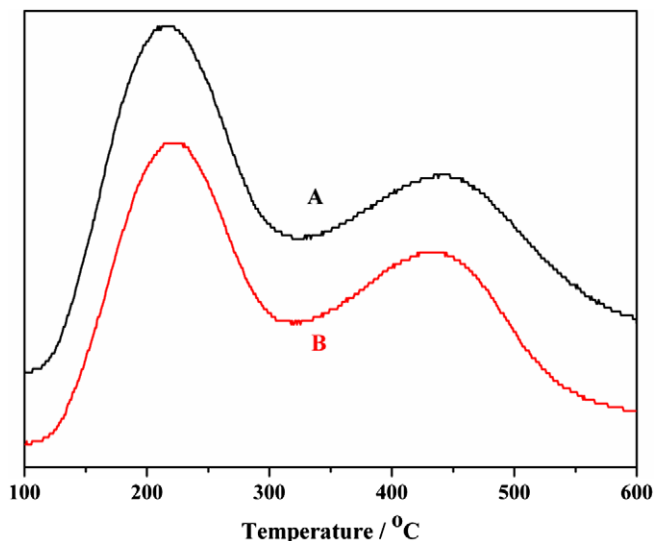


Fig. 12. NH_3 -TPD profiles of (A) H-8172-CB and (B) H-R72 catalysts.

reaction to evaluate the catalytic performance of the protonated zeolite samples of 8172-CB and R72. Fig. 11 depicts the catalytic activity observed in the isomerization of α -pinene on protonated 8172-CB and R72. The results show that the 8172-CB catalyst has much higher α -pinene conversion, no matter that 8172-CB and R72 catalysts have almost the same acidity (Fig. 12), while the $\text{SiO}_2/\text{Al}_2\text{O}_3$ ratio of 8172-CB and R72 is 26.7 and 29.5 determined by inductively coupled plasma atomic emission spectrum. These results show that the prepared ZSM-5 sample with hierarchical porosity of micro/meso/macro-pores offers perspective as an efficient catalyst in zeolite catalysis for its improved transport properties. Potentially the strategy demonstrated in this work could be used for the design and fabrication of industrial zeolite catalysts with high activity.

4. Conclusions

In the current work, we have successfully prepared columned ZSM-5 monoliths with mesoporous and macroporous structures by hydrothermal transformation of the β zeolite-containing precursors. The formation of hollow structure is contributed to the dissolution of β zeolite and the crystallization of the adding aluminosilicate into outer ZSM-5 crystals in high alkalinity synthesis conditions. The ZSM-5 monoliths prepared here have uniform cylindrical macroscopic morphologies and excellent mechanical strength due to the intergrowth of zeolite, which may have much effective surface area and better catalytic property. As a facile approach, hydrothermal transformation of pre-formed extrudates of aluminosilicate could lead to the mass production of zeolite monoliths with uniform morphology and hierarchical structure.

Acknowledgement

This work was supported by the NSFC (20890122 and 20721063), the STCSM (08251203000 and 09DZ2271500), 863 programme

(2009AA033701) and the Major State Basic Research Development Program of China (2009CB623502 and 2009CB623506).

References

- [1] D.W. Breck, *Zeolites and Molecular Sieves*, Wiley, New York, 1974.
- [2] M.E. Davis, *Nature* 417 (2002) 813.
- [3] D.J. Wang, Z.N. Liu, X.L. Li, Z.K. Xie, *Prog. Chem.* 20 (2008) 637.
- [4] S. Bernasconi, J.A. van Bokhoven, F. Krumeich, G.D. Pirngruber, R. Prins, *Microporous Mesoporous Mater.* 66 (2003) 21.
- [5] J.C. Groen, L.A.A. Peffer, J.A. Moulijn, J. Pérez-Ramírez, *Chem. Eur. J.* 11 (2005) 4983.
- [6] M. Choi, H.S. Cho, R. Srivastava, C. Venkatesan, D.-H. Choi, R. Ryoo, *Nat. Mater.* 5 (2006) 718.
- [7] C.J.H. Jacobsen, C. Madsen, J. Houzvicka, I. Schmidt, A. Carlsson, *J. Am. Chem. Soc.* 122 (2000) 7116.
- [8] B.T. Holland, L. Abrams, A. Stein, *J. Am. Chem. Soc.* 121 (1999) 4308.
- [9] Y.J. Wang, Y. Tang, Z. Ni, W.M. Hua, W.L. Yang, X.D. Wang, W.C. Tao, Z. Gao, *Chem. Lett.* 29 (2000) 510.
- [10] K.H. Rhodes, S.A. Davis, F. Caruso, B. Zhang, S. Mann, *Chem. Mater.* 12 (2000) 2832.
- [11] D.J. Wang, G.B. Zhu, Y.H. Zhang, W.L. Yang, B.Y. Wu, Y. Tang, Z.K. Xie, *New J. Chem.* 29 (2005) 272.
- [12] V. Valtchev, *Chem. Mater.* 14 (2002) 4371.
- [13] A.G. Dong, Y.J. Wang, Y. Tang, N. Ren, Y.H. Zhang, Z. Gao, *Chem. Mater.* 124 (2002) 3217.
- [14] A.G. Dong, Y.J. Wang, D.J. Wang, W.L. Yang, Y.H. Zhang, N. Ren, Z. Gao, Y. Tang, *Microporous Mesoporous Mater.* 64 (2003) 69.
- [15] J.C. Groen, T. Bach, U. Ziese, A.M. Paulaime-van-Donk, K.P. de Jong, J.A. Moulijn, J. Pérez-Ramírez, *J. Am. Chem. Soc.* 127 (2005) 10792.
- [16] C.S. Mei, Z.C. Liu, P.Y. Wen, Z.K. Xie, W.M. Hua, Z. Gao, *J. Mater. Chem.* 18 (2008) 3496.
- [17] Y.R. Wang, M. Lin, A. Tuel, *Microporous Mesoporous Mater.* 102 (2007) 80.
- [18] W.C. Li, A.H. Lu, R. Palkovits, W. Schmidt, B. Spliethoff, F. Schüth, *J. Am. Chem. Soc.* 127 (2005) 12595.
- [19] D.J. Wang, Z.N. Liu, W.M. Hua, Z.K. Xie, *Petrochem. Tech.* 36 (2007) 1061.
- [20] H.T. Wang, L.M. Huang, Z.B. Wang, A. Mitra, Y.S. Yan, *Chem. Commun.* (2001) 1364.
- [21] L. Tosheva, B. Mihailova, V. Valtchev, J. Sterte, *Microporous Mesoporous Mater.* 48 (2001) 31.
- [22] Y.-J. Lee, J.S. Lee, Y.S. Park, K.B. Yoon, *Adv. Mater.* 13 (2001) 1259.
- [23] V. Valtchev, *J. Mater. Chem.* 12 (2002) 1914.
- [24] V. Valtchev, M. Smahli, A.C. Faust, L. Vidal, *Angew. Chem. Int. Ed.* 42 (2003) 2782.
- [25] A.G. Dong, Y.J. Wang, Y. Tang, Y.H. Zhang, N. Ren, Z. Gao, *Adv. Mater.* 14 (2002) 1506.
- [26] Y.J. Wang, F. Caruso, *Adv. Funct. Mater.* 14 (2004) 1012.
- [27] S. Mintova, M. Hözl, V. Valtchev, B. Mihailova, Y. Bouizi, T. Bein, *Chem. Mater.* 16 (2004) 5452.
- [28] G. Majano, S. Mintova, O. Ovsitser, B. Mihailova, T. Bein, *Microporous Mesoporous Mater.* 80 (2005) 227.
- [29] D.J. Wang, Z.N. Liu, Z.K. Xie, *J. Inorg. Chem.* 23 (2008) 592.
- [30] J.C. Groen, S. Abelló, L.A. Villaescusa, J. Pérez-Ramírez, *Microporous Mesoporous Mater.* 114 (2008) 93.
- [31] R. Ravishanker, C.E.A. Kirschhock, B.J. Schoeman, P. Vannopen, P.J. Grobet, S. Storck, W.F. Maier, J.A. Martens, F.C. De Schryver, P.A. Jacobs, *J. Phys. Chem. B* 102 (1998) 2633.
- [32] Y.C. Tong, T.B. Zhao, F.Y. Li, Y. Wang, *Chem. Mater.* 18 (2006) 4218.
- [33] H.T. Wang, Z.B. Wang, L.M. Huang, A. Mitra, B. Holmberg, Y.S. Yan, *J. Mater. Chem.* (2001) 2307.
- [34] B.T. Holland, *Microporous Mesoporous Mater.* 89 (2006) 291.
- [35] S.I. Zones, Y. Nakagawa, *Microporous Mater.* 2 (1994) 543.
- [36] R.K. Ahedi, Y. Kubota, Y. Sugi, *J. Mater. Chem.* (2001) 2922.
- [37] C. Zenonos, G. Sankar, J. García-Martínez, A. Aliev, A.M. Beale, *Catal. Lett.* 86 (2003) 279.
- [38] C.S. Cundy, P.A. Cox, *Microporous Mesoporous Mater.* 82 (2005) 1.
- [39] B.C. Lipens, J.H. de Boer, *J. Catal.* 4 (1965) 319.